ORGANIC CHEMISTRY

10.1126/sciadv.1500390

Near-IR squaraine dye–loaded gated periodic mesoporous organosilica for photo-oxidation of phenol in a continuous-flow device

Parijat Borah,[1]* Sivaramapanicker Sreejith,[1]* Palapuravan Anees,[2]* Nishanth Venugopal Menon,[3] Yuejun Kang,[3] Ayyappanpillai Ajayaghosh,[2†] Yanli Zhao[1,4†]

Periodic mesoporous organosilica (PMO) has been widely used for the fabrication of a variety of catalytically active materials. We report the preparation of novel photo-responsive PMO with azobenzene-gated pores. Upon activation, the azobenzene gate undergoes *trans-cis* isomerization, which allows an unsymmetrical near-infrared squaraine dye (Sq) to enter into the pores. The gate closure by *cis-trans* isomerization of the azobenzene unit leads to the safe loading of the monomeric dye inside the pores. The dye-loaded and azobenzene-gated PMO (Sq-azo@PMO) exhibits excellent generation of reactive oxygen species upon excitation at 664 nm, which can be effectively used for the oxidation of phenol into benzoquinone in aqueous solution. Furthermore, Sq-azo@PMO as the catalyst was placed inside a custom-built, continuous-flow device to carry out the photo-oxidation of phenol to benzoquinone in the presence of 664-nm light. By using the device, about 23% production of benzoquinone with 100% selectivity was achieved. The current research presents a prototype of transforming heterogeneous catalysts toward practical use.

INTRODUCTION

Periodic mesoporous organosilica (PMO) prepared by the polycondensation of small hydrocarbon-bridged silane molecules has been proven to be a promising material for various applications including catalysis (*1*–*4*). Relatively hydrophobic nanoconfinement inside the mesopores inherited from the hydrocarbon bridges makes PMO a suitable porous domain for hosting a variety of organic molecules in solution (*1*). During the past decades, several mechanized, mesoporous silica materials were fabricated and successfully used to entrap different cargos inside the mesopores for controlled release. In addition, various stimuli-responsive, gated mesoporous silica materials were achieved by adopting different synthetic pathways of surface modifications (*5*–*8*). Among these gated materials, photothermal triggered systems can be considered clean-energy powered systems on account of the reversible mode of operation without by-products. For instance, Mal *et al.* reported coumarin-functionalized, MCM-41–type, mesoporous silica material and demonstrated its uptake, storage, and release of organic molecules through photo-controlled reversible dimerization of coumarin derivatives (*9*). Apart from coumarin, azobenzene and its derivatives were also proven as photo-switchable gates for mesoporous materials, and some azobenzene-assisted photothermal-powered mesoporous systems were successfully used in the areas of controlled cargo loading and release (*10*).

The chemical modification of the organic bridges in PMO has been considered a very effective approach to achieve highly functionalized pores with uniform mesopore space. Covalently bonded organic bridges such as phenylene and ethenylene units in the siloxane network of PMO can be functionalized chemically via direct sulfonation (*11*), bromination (*12*), amination (*13*, *14*), hydroxylation (*15*), and Diels-Alder reaction (*16*). Among these transformations, direct amination is advantageous, because the amino functional group offers the versatility for further modifications via amide, imine, urea, and diazo bond formations. Ohashi *et al.* successfully demonstrated the direct amination of phenylene bridges in the mesoporous benzene-silica network of PMO via a two-step chemical transformation (*14*). This methodology becomes more significant for the preparation of switchable gate–functionalized PMO nanomaterials. For the design of switchable organic gates, azobenzene and its derivatives are commonly used because of their unique *cis-trans* isomerization properties upon alternate treatment with ultraviolet/visible light (UV/Vis) irradiation or heat.

Inspired by the unique features of PMO and azobenzene, we developed an approach to functionalize azobenzene moieties directly onto the phenylene bridges of a benzene-PMO by using the post-synthetic amination methodology. Here, the azobenzene-appended benzene-PMO (denoted as *trans*-azo@PMO) obtained serves as a nanocontainer with hydrophobic confinement, in which the azobenzene units in the pores perform the functions of (i) photo-responsive gates to tune the internal pore size of PMO and (ii) spacers to prevent guest molecules from undesired aggregation.

We selected a squaraine derivative as the guest molecule. Squaraine (Sq) dyes are a class of zwitterionic dyes that exhibit excellent photophysical properties in the near-infrared (NIR) region and serve as efficient photosensitizers to produce singlet oxygen ($^1O_2$) (*17*–*21*). This fascinating class of dyes has also been proven to be potential candidates in various applications such as metal ion sensing (*22*–*24*), NIR fluorescent labeling (*25*), two-photon absorption (*26*, *27*), and the detection of amino thiols in blood plasma (*28*–*30*). Recently, we and others have demonstrated different strategies to protect Sq dyes from nucleophilic attack for effective utilization (*31*–*33*).

In azo@PMO, the opening and closure of the gate were reversibly controlled by light-induced *cis-trans* isomerization of azobenzene

[1]Division of Chemistry and Biological Chemistry, School of Physical and Mathematical Sciences, Nanyang Technological University, 21 Nanyang Link, 637371 Singapore, Singapore. [2]Photosciences and Photonics Group, Chemical Sciences and Technology Division, Council of Scientific and Industrial Research–National Institute for Interdisciplinary Science and Technology, Trivandrum 695019, India. [3]School of Chemical and Biomedical Engineering, Nanyang Technological University, 62 Nanyang Drive, 637459 Singapore, Singapore. [4]School of Materials Science and Engineering, Nanyang Technological University, 50 Nanyang Avenue, 639798 Singapore, Singapore.
*These authors contributed equally to this work.
†Corresponding author. Email: ajayaghosh@niist.res.in (A.A.); zhaoyanli@ntu.edu.sg (Y.Z.)

units. An unsymmetrical NIR Sq dye was loaded inside open pores as the guest molecule when the azobenzene gate was at its *cis* conformation. The azobenzene gate was then closed through its *cis-trans* isomerization under visible light irradiation, allowing the loaded Sq to be intercalated by the *trans*-azobenzene spacers in the pores without the formation of Sq aggregates. The dye-loaded hybrid (Sq-*trans*-azo@PMO) could act as a photosensitizer, exhibiting the capability to generate reactive oxygen species upon light excitation at 664 nm (Fig. 1). Finally, Sq-*trans*-azo@PMO was used as a catalytic bed in a microfluidic free-flow device, where the photo-oxidation of phenol to benzoquinone (BQ) with a constant conversion yield was carried out.

RESULTS

First, we prepared a phenylene-bridged PMO (denoted as Ph-PMO) by adopting an established synthesis route (*34*). During the preparation, we selected a pluronic P123 surfactant as the template to achieve a pore size of more than 5 nm under acidic conditions. Then, the prepared Ph-PMO was subjected to a nitration process to generate nitro Ph-PMO (denoted as Ph-PMO-NO_2), followed by a reduction to generate amino functionality in PMO (denoted as Ph-PMO-NH_2, fig. S1). After the successful preparation of Ph-PMO-NH_2, an azobenzene compound (compound 4 in fig. S2) was grafted through amide coupling, leading to *trans*-azo@PMO for further uses. Ph-PMO has a relatively higher hydrophobic environment inside the pore channels according to previous reports (*35*–*37*). The functionalization of the azobenzene group with a terminal ethoxy unit presumably reinforces the internal hydrophobicity of the pore channels. In addition, direct amination onto the phenylene bridges could facilitate further grafting of the azobenzene unit.

Successful functionalization was characterized by Fourier transform infrared spectroscopy (FT-IR), ^{13}C cross-polarization magic angle spinning nuclear magnetic resonance (CP-MAS NMR), and ^{29}Si CP-MAS NMR techniques (see the Supplementary Materials for more details). The analytical results obtained indicate the successful reduction of $-NO_2$ to $-NH_2$ functionality to form Ph-PMO-NH_2, followed by the introduction of the azobenzene derivative through amide linkage.

UV/Vis absorption studies (Fig. 2) were carried out to obtain an insight into the photothermal response of azo@PMO in aqueous solution. The UV/Vis absorption spectrum of Ph-PMO-NH_2 exhibits broad scattering in water with a maximum of 320 nm corresponding to the phenyl unit in the PMO skeleton (Fig. 2A). Similarly, *trans*-azo@PMO in water presents a signature absorption peak at 380 nm corresponding to the π-π^* transition of the azobenzene unit (Fig. 2A). The irradiation of *trans*-azo@PMO under 380-nm light for 20 min shows a decrease in the absorption intensity at 380 nm, with concomitant formation of a new band at 460 nm corresponding to the *cis* isomer, that is, *cis*-azo@PMO (Fig. 2A). Furthermore, we demonstrated the reversible process of the *trans-cis* isomerization between *trans*-azo@PMO and *cis*-azo@PMO up to six cycles (Fig. 2B), proving the efficient *trans-cis* isomerization capability of azo@PMO in aqueous solution.

We then synthesized an unsymmetrical Sq dye by coupling half-squaraine with dimethoxy styrylpyrrole under azeotropic refluxing conditions in benzene/butanol (fig. S3). The dye was purified by column

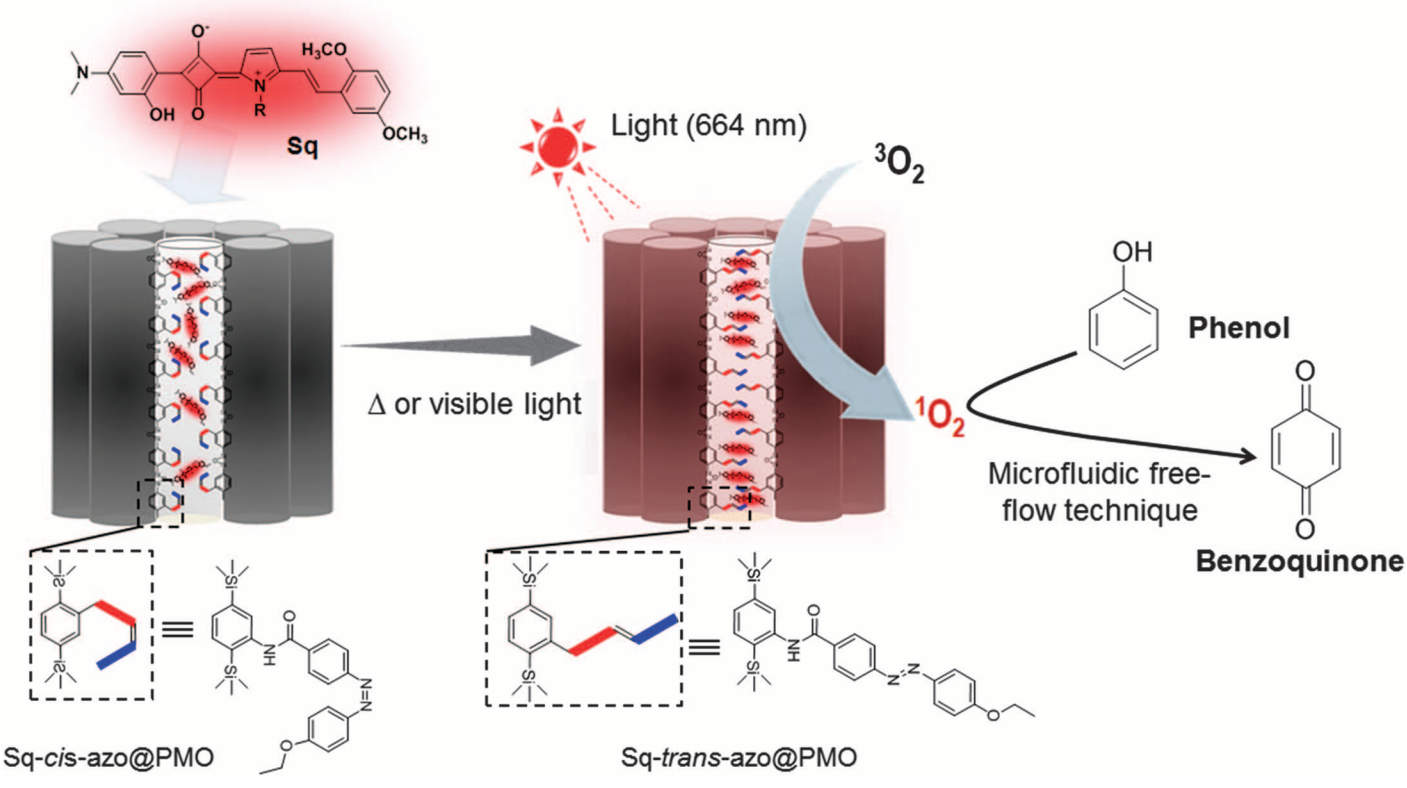

Fig. 1. Schematic representation of the preparation and $^1O_2$ generation of Sq-azo@PMO. Overall process for the preparation of Sq-azo@PMO and its capability for the photo-oxidation of phenol in water.

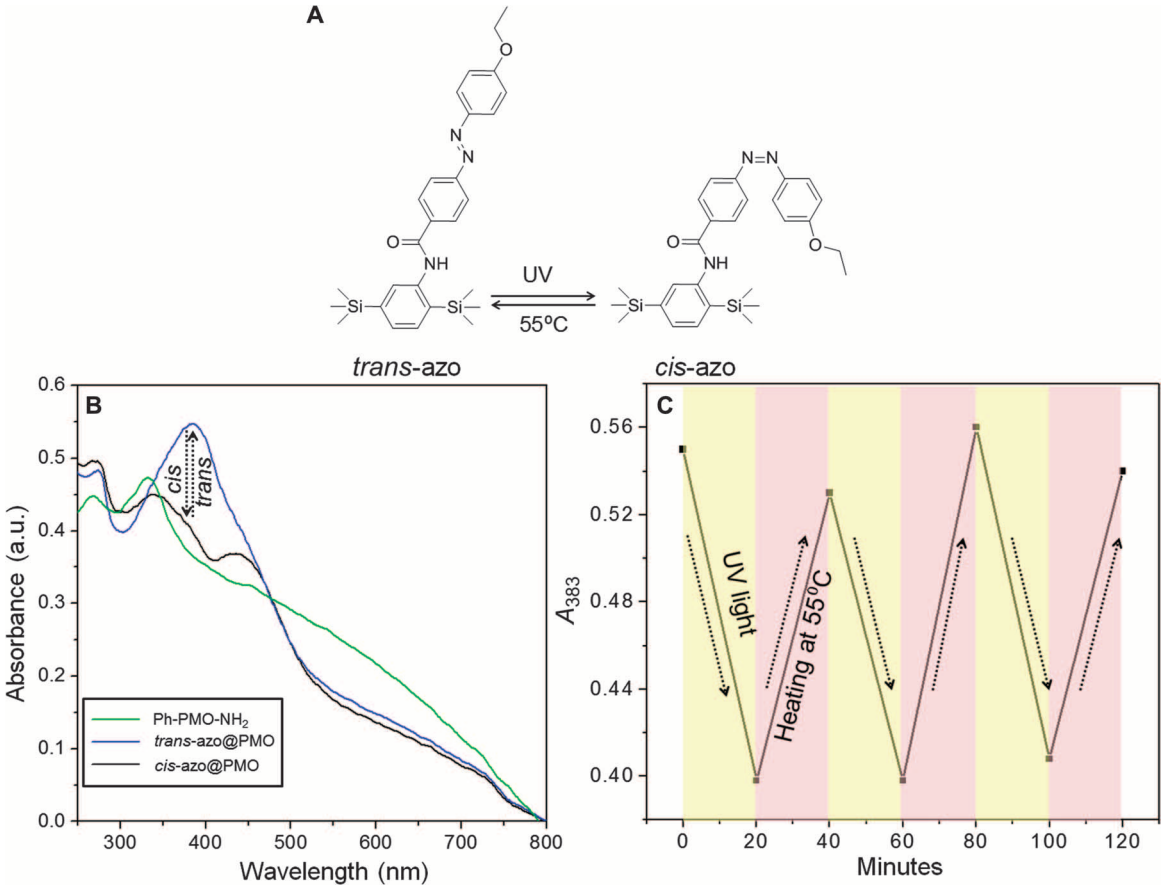

Fig. 2. Photoisomerization of azo@PMO. (**A**) Schematic representation of reversible isomerization between *trans*-azo@PMO and *cis*-azo@PMO under light irradiation and heat. a.u., absorbance units. (**B**) UV/Vis absorption spectra of Ph-PMO-NH_2, *cis*-azo@PMO, and *trans*-azo@PMO (1.5 mg ml^{-1} in aqueous solution). The changes in the UV/Vis absorption spectra due to the isomerization of *trans*-azo@PMO to *cis*-azo@PMO (1.5 mg ml^{-1}) were recorded under the irradiation of 383-nm UV light for 20 min. (**C**) Absorbance changes of the UV/Vis spectra of azo@PMO at 383 nm as a function of cycles upon alternating UV light irradiation and heating at 55°C.

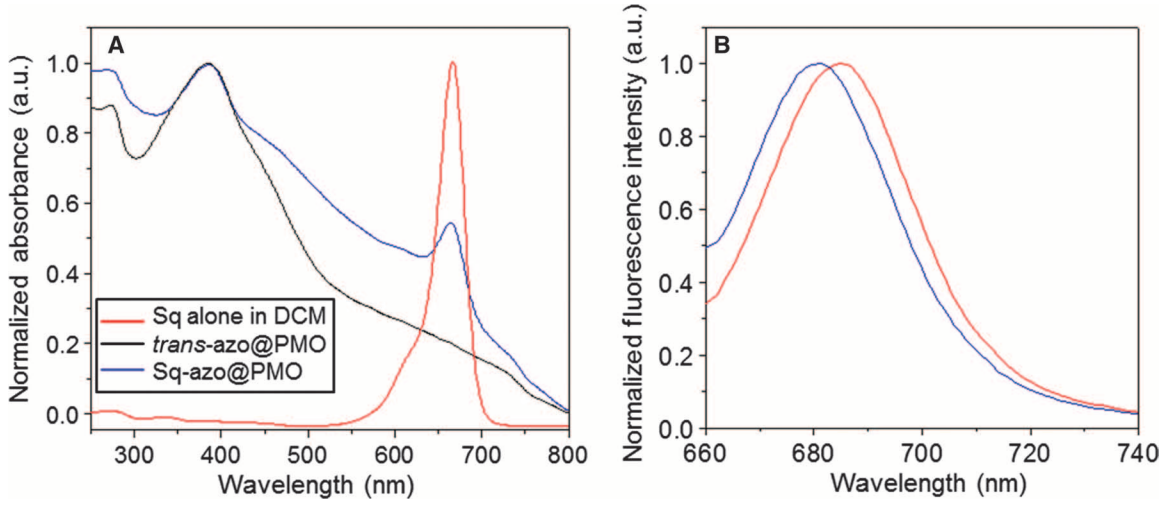

Fig. 3. Photophysical studies of Sq-azo@PMO. (**A**) UV/Vis absorption spectra of Sq in dichloromethane (DCM) (red curve), *trans*-azo@PMO in water (black curve), and Sq-azo@PMO in water (blue curve). (**B**) Emission spectra of Sq in DCM (red curve) and Sq-azo@PMO in water (blue curve).

chromatography over silica gel and characterized by ^{1}H NMR, ^{13}C NMR, and high-resolution mass spectrometry. Sq exhibits a characteristic absorption maximum at 667 nm ($\varepsilon = 165{,}620\ M^{-1}\ cm^{-1}$, Fig. 3A) and a corresponding emission maximum at 685 nm (Fig. 3B) in dichloromethane.

The synthesized Sq was subsequently loaded inside azo@PMO to generate the final gated hybrid (Sq-*trans*-azo@PMO or Sq-azo@PMO). The loading procedure is described in Materials and Methods. Furthermore, the amount of Sq loaded in Sq-azo@PMO was determined by thoroughly extracting all dye molecules from the pores in dichloromethane under UV light irradiation to open the gates (fig. S8). All the extracted Sq dye in dichloromethane solution was quantified by its UV/Vis absorbance intensity and was calculated to be about 0.2 wt %.

Transmission electron microscope (TEM) images of Ph-PMO, Ph-PMO-NH_2, *trans*-azo@PMO, and Sq-azo@PMO are shown in Fig. 4. In the case of Ph-PMO, mesopores having a diameter of ~6 nm are uniformly arranged in honeycomb-like hexagonal arrays throughout the sample (Fig. 4A). The image also indicates a wall thickness of ~3 nm (fig. S9A). Upon subsequent modifications, the regular mesoporous structure of pristine Ph-PMO was basically preserved in Ph-PMO-NH_2 and *trans*-azo@PMO (Fig. 4, B and C). However, after the loading of Sq dye, the contrast between the pore channels and the pore walls markedly decreased because of the intercalation of the dye molecules inside the pores (Fig. 4D and fig. S10, A and B). The TEM images of *trans*-azo@PMO obtained after the removal of Sq from Sq-azo@PMO also show a regular mesoporous structure, indicating the retention of mesostructure in Sq-azo@PMO (fig. S10, C and D) with a constant wall thickness (fig. S9B). These textural observations for the four phases of PMOs are in agreement with the results obtained from the N_2 adsorption/desorption measurements shown below.

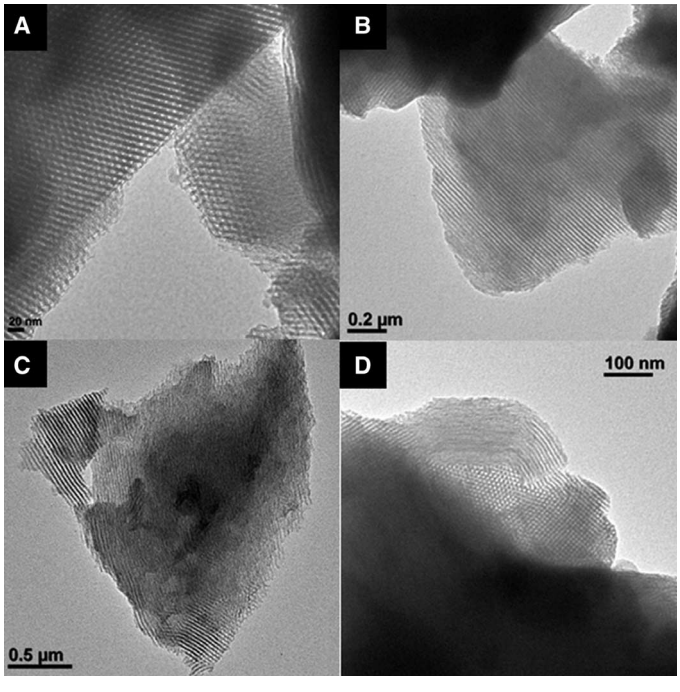

Fig. 4. TEM images of PMOs. (**A** to **D**) TEM images of (A) Ph-PMO, (B) Ph-PMO-NH_2, (C) *trans*-azo@PMO, and (D) Sq-azo@PMO.

We performed isothermal N_2 adsorption/desorption measurements for Ph-PMO, Ph-PMO-NH_2, *trans*-azo@PMO, and Sq-azo@PMO to determine their surface areas and pore size distributions (Table 1). From the N_2 adsorption isotherms under the lowest pressure, the Brunauer-Emmett-Teller (BET) method was used to calculate the specific surface areas of the materials, whereas we adopted the nonlocal density functional theory (NLDFT) equilibrium model for cylindrical pores, considering N_2 as an adsorbate and silica as an adsorbent at 77 K to achieve the pore size distributions of the PMOs. We found that Ph-PMO, Ph-PMO-NH_2, *trans*-azo@PMO, and Sq-azo@PMO showed typical type IV isotherms with different kinds of adsorption hysteresis. Ph-PMO and Ph-PMO-NH_2 exhibited typical H1 hysteresis, indicating the presence of a mesoporous matrix with uniform pore distribution (fig. S11, A and B) (*38*). However, the surface modification in the case of Ph-PMO-NH_2 reduced its surface area and the pore size (Table 1). On the other hand, the functionalization of the azobenzene unit led to a marked reduction in the pore diameter and surface area for *trans*-azo@PMO, offering an isotherm with H3 type hysteresis (fig. S11C) (*38*). Upon the loading of Sq dye into the pores of *trans*-azo@PMO, the resulting Sq-azo@PMO underwent further reduction of both surface area and pore size. The N_2 isotherm of Sq-azo@PMO was also assigned to type IV isotherm without any distinguishable adsorption hysteresis (fig. S11D), indicating that the loaded dye occupies the mesoporous channels.

To understand the photophysical properties of the prepared hybrids, UV/Vis absorption and fluorescence spectroscopy studies were carried out. In the UV/Vis absorption spectra, we observed that the aqueous suspension of Sq-azo@PMO exhibits a characteristic peak at ~380 nm corresponding to the *trans*-azobenzene moiety and a peak around 664 nm assigned to the dye intercalated inside the pores (Fig. 3A). As compared to the absorption of Sq in dichloromethane (Fig. 3A), Sq-azo@PMO shows no obvious change of the absorption maximum at 664 nm in aqueous solution. Sq-azo@PMO reveals an ~5-nm blue shift of the emission maximum at 680 nm under excitation at 650 nm when compared to that of Sq in dichloromethane (Fig. 3B). The observed blue shift in the emission maximum could be attributed to the internal absorption by the hydrophobic interior of the azobenzene-intercalated PMO pores. Hence, it was proven that the azobenzene unit grafted in the pore wall of PMO serves as not only a closed gate in its *trans*-form but also a spacer between Sq molecules to effectively prevent Sq aggregation inside the pores. Furthermore, the UV/Vis spectrum of Sq-azo@PMO showed a decrease in the absorption intensity at 380 nm in aqueous suspension after 380-mn UV irradiation for 30 min on account of the formation of Sq-*cis*-azo@PMO (fig. S12). However, the absorption maximum at 664 nm corresponding to the Sq dye disappeared in the case of Sq-*cis*-azo@PMO (fig. S12). The open pores of Sq-*cis*-azo@PMO were not able to protect the trapped Sq from

Table 1. Textural and porosity data of different PMOs.

No.	PMO	BET ($m^2\ g^{-1}$)	Pore diameter (nm)
1	Ph-PMO	1078	6.2
2	Ph-PMO-NH_2	727	3.7
3	*trans*-azo@PMO	544	2.5
4	Sq-azo@PMO	470	1.7

aggregation under the hostile aqueous environment due to the formation of *cis*-azobenzene isomer. Thus, aggregated Sq lost its photophysical properties in aqueous solution. These observations provide solid evidence in support of the role of an azobenzene unit as the gate in azo@PMO.

Furthermore, we investigated the photo-induced $^1O_2$ generation capability of the Sq-azo@PMO hybrid through an indirect chemical method using 9,10-anthracenediyl-bis-(methylene)dimalonic acid (ADMA) as the $^1O_2$ trap (*39*). ADMA reacts with $^1O_2$ to produce corresponding endoperoxide that can be monitored by the absorption changes of ADMA. An aqueous solution of ADMA (8.2×10^{-5} M) was mixed with an aqueous suspension of Sq-azo@PMO (0.3 mg ml^{-1}) under stirring. A typical absorption spectrum of the mixture shows two characteristic regions (fig. S13), that is, the sharp absorption corresponding to ADMA at 350 to 415 nm and the absorption of Sq from 630 to 700 nm. Upon the irradiation of 664-nm light for 50 min, the absorption of ADMA decreased continuously (fig. S14A). The distinct photobleaching of ADMA indicates the photo-induced generation of $^1O_2$ by monomeric Sq protected inside Sq-azo@PMO in aqueous medium. In addition, the $^1O_2$ quantum yield of Sq-azo@PMO was calculated to be 9.9% (see the Experimental Section in the Supplementary Materials for more details). In another control experiment, the same concentration of ADMA aqueous solution containing *trans*-azo@PMO was irradiated by 664-nm light to check the photo-induced $^1O_2$ generation capability of *trans*-azo@PMO without Sq. No photo-induced $^1O_2$ generation was observed after the light irradiation for 60 min (fig. S14B). Therefore, effective $^1O_2$ generation of Sq-azo@PMO in aqueous condition provides a proof of concept for protecting Sq dye in its monomeric state inside mesoporous channels of PMO to preserve its photophysical properties for further applications.

Among various applications of $^1O_2$, using $^1O_2$ as a reactive reagent for the synthesis of fine chemicals and the treatment of wastewater has attracted a lot of attention. Phenol and its derivatives are toxic compounds commonly found in the wastewater produced from paper and dye manufacturing industries as well as oil refineries because of their resistance to biodegradation. One common approach of dealing with such water contaminants is to oxidize them into corresponding oxygenated compounds that are easily biodegradable (*9*, *36*, *37*). Many studies have demonstrated the oxidation of phenol and its derivatives in organic solvents through in situ generation of $^1O_2$ in the presence of photosensitizers such as eosin, rose bengal, methylene blue, riboflavin, and Zn(II) tetraphenylporphyrin (*40*, *41*). Similar reactions have also been carried out in aqueous solution using various dyes and metal complexes as the photosensitizers, and it was evident that the presence of monomeric photosensitizers in

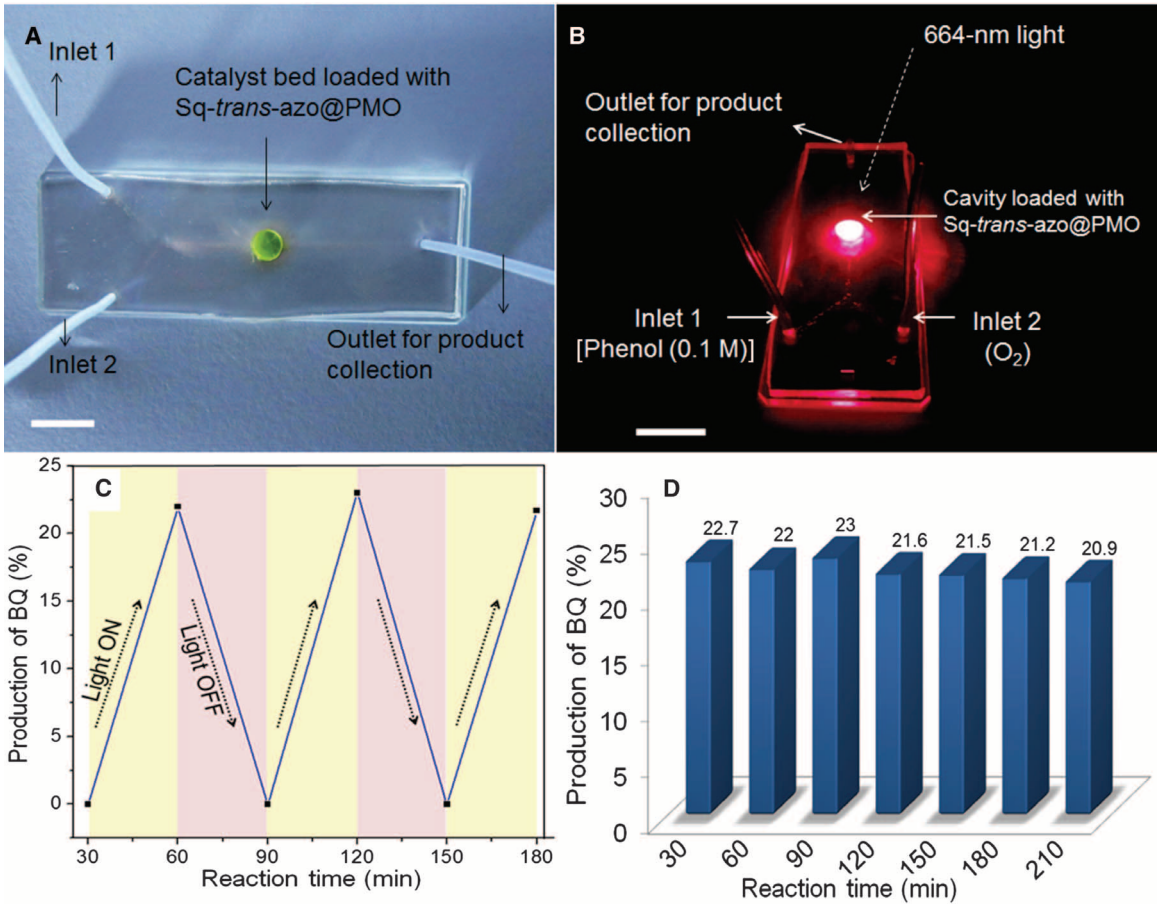

Fig. 5. Microfluidic free-flow device loaded with Sq-azo@PMO for photo-oxidation of phenol. (**A**) Photograph of the microfluidic device under normal light. (**B**) Operational mode of Sq-azo@PMO loaded microreactor under the irradiation of 664-nm light. Scale bar, 1 cm. (**C** and **D**) Photo-oxidation of phenol inside the microfluidic channel as a function of cycles upon (C) alternating irradiation of light and (D) continuous irradiation of light.

solution is critical to achieve the highest efficacy (*41*). However, most of the organic dyes undergo severe aggregation in the aqueous medium, which substantially decreases their ability to generate $^1O_2$ for practical applications.

In this context, we carried out the oxidation of phenol to BQ using $^1O_2$ generated from Sq-azo@PMO under 664-nm light irradiation in aqueous medium (Fig. 1). The main challenges associated with this method that we encountered were (i) how to reduce the reaction time to achieve 100% conversion of phenol into BQ because a slow rate of conversion as well as a rapid decline in conversion rate were observed as the reaction proceeded (fig. S15) and (ii) how to address the limitation over the area for light irradiation. It is also important to mention that $^1O_2$ exhibits a short half-life (0.6 μs) and a short diffusion distance (0.1 μm) in aqueous medium (*41*), for which efficient utilization of this reactive oxygen species is a great challenge, especially in macroscale. As an approach to circumventing the abovementioned issues, we used a microfluidic device that has a short diffusion time for the reactants, which contributes to the improved mass transportation in the reactor (*42*). For this purpose, we designed and fabricated a two-inlet–single-outlet "Y"-type microfluidic device (fig. S16) to carry out the free-flow photo-oxidation of phenol using Sq-azo@PMO. Figure 5A shows the photograph of the ready-to-use microfluidic device fitted with two inlets that allow the inputs of aqueous phenol solution (0.1 M) and oxygen. A central chamber was designed to load the catalyst and was later filled with Sq-azo@PMO (3 mg). To investigate the photo-oxidation of phenol to BQ, an optimized condition was used after several trial experiments. Basically, aqueous solution of phenol (0.1 M) was allowed to flow through inlet 1 using a syringe pump at a rate of 2 ml hour^{-1}. O_2 was simultaneously flowed through inlet 2 under 1-atm pressure. The central catalytic bed was then irradiated by 664-nm light (2.5 mW cm^{-2}) to generate $^1O_2$ in situ. Keeping a constant flow of both reactants, we carried out the oxidation reaction at room temperature upon the irradiation of a laser light with a wavelength of 664 nm (Fig. 5B). The products were collected from the outlet every 30 min.

The flame ionization detector gas chromatography (FID-GC) analysis indicates that the photo-oxidation could lead to a selective conversion of phenol to BQ. The microfluidic device–based microreactor showed 22 to 23% yield of the BQ formation during every cycle of the reaction under the irradiation of 664-nm light for 30 min each cycle (Fig. 5D). The yield is about 1.5 times higher than that obtained from a cuvette-based aqueous phase reaction, for a reaction time of 30 min. Furthermore, we investigated the effect of light by carrying out a periodic switch "on" and "off" process, proving that an effective oxidation process takes place only in the presence of light (Fig. 5C). The reaction was further investigated under the same microfluidic conditions with continuous irradiation of light for longer reaction time, and the products were collected and analyzed periodically. The results showed that, for every 30 min of reaction under the given conditions up to a total of 210 min, a consistent production of BQ with 21 to 23% yield was obtained (Fig. 5B), whereas a rapid declination of the BQ production was observed in the cuvette-based aqueous phase reaction (fig. S15). After the oxidation reaction, the used Sq-azo@PMO was recovered, and its photophysical properties were analyzed by UV/Vis spectroscopy. After comparing the spectra of Sq-azo@PMO before and after the photo-oxidation, it could be concluded that the loaded Sq dye remains stable in its monomeric state for a long time in an aqueous environment, after the generation of $^1O_2$ (fig. S17). In another control experiment, we performed the photo-oxidation reaction in a microfluidic device using Sq-loaded benzene-PMO (Sq@PhPMO) as the catalytic bed under the same conditions [see the Supplementary Materials (fig. S18) for the details on preparation and characterization]. However, no production of BQ was observed. This observation validates the necessity of monomeric Sq for achieving the catalytic activity. It also proves that only gated PMO, that is, *trans*-azo@PMO, can prevent the unwanted aggregation of Sq in aqueous medium.

DISCUSSION

Here, we have reported the development of azobenzene gate–appended phenylene-bridged PMO (azo@PMO). The azobenzene moieties inside the pores serve as the gates of the mesoporous channels, which can be reversibly closed and opened by virtue of *trans-cis* isomerization under light irradiation. The photo-responsive gate functionalized inside the pore channels of PMO has been less investigated in the literature because of the unavailability of suitable synthetic approaches. We have adopted a post-synthetic grafting method to introduce an azobenzene unit inside the pore channels. The obtained azo@PMO has unique properties capable of loading and releasing cargos in a light-controlled manner. Thus, an unsymmetrical Sq dye has been loaded inside the gated pores in its monomeric state because of the intercalation of *trans*-azobenzene spacers, leading to the formation of the Sq-azo@PMO hybrid. The monomeric Sq inside the mesoporous channels of azo@PMO shows high efficiency to generate $^1O_2$ in an aqueous environment upon light irradiation. To efficiently use the generated $^1O_2$ in situ, a microfluidic reactor loaded with Sq-azo@PMO has been fabricated, where the photo-oxidation of phenol to BQ has been carried out. By using the microfluidic reactor, up to 23% production of BQ with 100% selectivity has been achieved. Thus, the current research presents the first gated heterogeneous catalyst and paves the way for applying such gated catalysts within microfluidic reactors toward practical uses.

MATERIALS AND METHODS

Preparation of Sq-azo@PMO

In a typical process, *trans*-azo@PMO (20 mg) was suspended in acetonitrile (10 ml), and the suspension was stirred under UV light with a wavelength of 380 nm for 1 hour to convert surface-functionalized azobenzene units from the *trans* form to the *cis* form. The photostationary state of the *cis*-azobenzene unit was confirmed by UV/Vis absorption. An Sq solution in acetonitrile (0.4 mM, 5 ml) was added to this suspension under UV light irradiation for 15 min. Subsequently, the mixture was stirred at 55°C under visible light for 2 hours. Solid material was isolated by centrifugation and thoroughly washed by acetonitrile followed by dichloromethane under sonication. The greenish blue material was dried in vacuum to generate Sq-azo@PMO.

Microfluidic chip fabrication

Soft lithography was used for the fabrication of polydimethylsiloxane (PDMS) chips. It involves two steps: the creation of a mold, followed by the creation of PDMS chips (*43*). The mold was created by photolithography, whereby a negative photoresist (SU-8 25, MicroChem

Inc.) was coated on a silicon substrate and exposed to UV radiation at 365 nm through a photomask. Once it was exposed, the substrate was baked and developed to obtain the final mold with a channel thickness of about 40 µm. PDMS (Sylgard 184, Dow Corning) was prepared by mixing an elastomer and a curing agent in a weight ratio of 10:1. Once PDMS was prepared, it was poured over the mold, and the curing was performed at 70°C for 2 hours, at the end of which PDMS was polymerized and the chip could be cut out from the mold.

Photo-oxidation of phenol in the microfluidic chip

Sq-azo@PMO (3 mg) was loaded into the cavity in the prepared microfluidic chip (fig. S16). A thin cotton plug was used in front of the outlet channel to prevent unwanted leakage of Sq-azo@PMO from the cavity. A microscopic cover glass was used to close the cavity using vacuum grease and transparent cello tape. The openings of the two inlets in the microfluidic chip were respectively connected to a syringe pump containing 0.1 M aqueous solution of phenol and to a balloon containing O_2 by using a plastic capillary tube with a 1-mm diameter. Likewise, the opening of the outlet was connected to a sample vial through a similar capillary tube to collect the reaction mixture after the reaction. The 0.1 M phenol solution was allowed to pass through the reactor cavity along with O_2 via a microchannel, at a continuous flow rate of 2 ml hour^{-1} with the help of the syringe pump. Under such reaction conditions, a laser light with a 664-nm wavelength was used to irradiate by focusing at the reactor cavity. The reaction mixture collected from the outlet was analyzed after an interval of 30 min. After determining the response factors for the reactant and product individually, the product and unreacted reactant were identified and quantified by using an Agilent 6890 GC system equipped with an FID.

SUPPLEMENTARY MATERIALS

Supplementary material for this article is available at http://advances.sciencemag.org/cgi/content/full/1/8/e1500390/DC1

Experimental section
Fig. S1. Synthetic route for two-step amination of Ph-PMO.
Fig. S2. Synthetic route for the preparation of azobenzene compounds.
Fig. S3. Synthetic route for Sq dye.
Fig. S4. Difference between consecutive absorbance at each time intervals was plotted against time for (a) the absorption decrease of ADMA upon the irradiation of 664 nm light by mixing with aqueous suspension of Sq-azo@PMO under stirring, and (b) the absorption decrease of ADMA upon the irradiation of 660 nm light by mixing with aqueous suspension of MB under stirring.
Table S1. EA results of various PMO materials.
FT-IR analyses of PMOs
Fig. S5. FT-IR spectra of (a) Ph-PMO, Ph- PMO-NO_2, and Ph-PMO-NH_2 as well as (b) *trans*-azo@PMO.
^{13}C CP-MAS NMR analyses of PMOs
Fig. S6. ^{13}C CP-MAS solid-state NMR spectra of Ph-PMO, Ph-PMO-NH_2, and *trans*-azo@PMO.
^{29}Si CP-MAS NMR analyses of PMOs
Fig. S7. ^{29}Si CP-MAS solid-state NMR spectra of (a) Ph-PMO-NH_2 and (b) *trans*-azo@PMO.
UV/Vis analyses of Sq-azo@PMO and azo@PMO
Fig. S8. UV/Vis spectra of (a) Sq-*trans*-azo@PMO measured after 48 hours of stirring in DCM and (b) azo@PMO obtained after the removal of Sq in DCM.
TEM images of Sq-azo@PMO and azo@PMO
Fig. S9. Wall thickness from TEM images of (a) Ph-PMO and (b) azo@PMO obtained after the removal of Sq from Sq-*trans*-azo@PMO.
Fig. S10. TEM images of (a and b) Sq-azo@PMO and (c and d) azo@PMO obtained after the removal of Sq from Sq-*trans*-azo@PMO.
N_2 adsorption/desorption measurements of PMOs
Fig. S11. Plots for N_2 adsorption/desorption isotherms with NLDFT pore size distribution (in the insets) of (a) Ph-PMO, (b) Ph-PMO-NH_2, (c) *trans*-azo@PMO, and (d) Sq-azo@PMO.
UV/Vis analysis of Sq-*trans*-azo@PMO and Sq-*cis*-azo@PMO
Fig. S12. UV/Vis absorption spectra of (a) Sq-*trans*-azo@PMO in water and (b) Sq-*cis*-azo@PMO obtained after irradiation of 383 nm UV light on Sq-*trans*-azo@PMO in water for 60 min.
Generation of $^1O_2$ by Sq-azo@PMO in aqueous medium
Fig. S13. UV/Vis absorption spectra of (a) ADMA in aqueous solution, (b) Sq-azo@PMO in aqueous suspension, and (c) ADMA along with Sq-azo@PMO in aqueous solution.
Fig. S14. UV/Vis absorption changes of ADMA aqueous solution in the presence of (a) Sq-azo@PMO and (b) *trans*-azo@PMO upon the irradiation of 664 nm light.
Photo-oxidation of phenol in aqueous medium
Fig. S15. Production of BQ as a function of time in cuvette-based aqueous phase.
Fig. S16. (a) Photograph of microfluidic channels, (b) loading of Sq-azo@PMO in the cavity, and (c) schematic representation of the cross-sectional view of the prepared microreactor.
UV/Vis analysis of Sq-azo@PMO before and after photo-oxidation reaction
Fig. S17. UV/Vis absorption spectra of Sq-azo@PMO in water (a) before the photo-oxidation reaction and (b) after recovered from the photo-oxidation reaction in a microfluidic reactor.
Preparation of Sq@PhPMO for control study
Fig. S18. UV/Vis absorption spectrum of Sq@PhPMO in water.
References (*44*–*46*)

REFERENCES AND NOTES

1. Q. Yang, J. Liu, L. Zhang, C. Li, Functionalized periodic mesoporous organosilicas for catalysis. *J. Mater. Chem.* **19**, 1945–1955 (2009).
2. N. Mizoshita, T. Tani, S. Inagaki, Syntheses, properties and applications of periodic mesoporous organosilicas prepared from bridged organosilane precursors. *Chem. Soc. Rev.* **40**, 789–800 (2011).
3. P. Borah, X. Ma, K. T. Nguyen, Y. Zhao, A vanadyl complex grafted to periodic mesoporous organosilica: A green catalyst for selective hydroxylation of benzene to phenol. *Angew. Chem. Int. Ed.* **51**, 7756–7761 (2012).
4. P. Borah, Y. Zhao, β-Diketimine appended periodic mesoporous organosilica as a scaffold for immobilization of palladium acetate: An efficient green catalyst for Wacker type reaction. *J. Catal.* **318**, 43–52 (2014).
5. Y. Chen, H. Chen, J. Shi, Drug delivery/imaging multifunctionality of mesoporous silica-based composite nanostructures. *Expert Opin. Drug Deliv.* **11**, 917–930 (2014).
6. C. Coll, A. Bernardos, R. Martínez-Máñez, F. Sancenón, Gated silica mesoporous supports for controlled release and signaling applications. *Acc. Chem. Res.* **46**, 339–349 (2013).
7. K. Ariga, A. Vinu, Y. Yamauchi, Q. Ji, J. P. Hill, Nanoarchitectonics for mesoporous materials. *Bull. Chem. Soc. Jpn.* **85**, 1–32 (2012.
8. M. W. Ambrogio, C. R. Thomas, Y.-L. Zhao, J. I. Zink, J. F. Stoddart, Mechanized silica nanoparticles: A new frontier in theranostic nanomedicine. *Acc. Chem. Res.* **44**, 903–913 (2011).
9. N. K. Mal, M. Fujiwara, Y. Tanaka, Photocontrolled reversible release of guest molecules from coumarin-modified mesoporous silica. *Nature* **421**, 350–353 (2003).
10. H. Yan, C. Teh, S. Sreejith, L. Zhu, A. Kwok, W. Fang, X. Ma, K. T. Nguyen, V. Korzh, Y. Zhao, Functional mesoporous silica nanoparticles for photothermal-controlled drug delivery in vivo. *Angew. Chem. Int. Ed.* **51**, 8373–8377 (2012).
11. S. Inagaki, S. Guan, T. Ohsuna, O. Terasaki, An ordered mesoporous organosilica hybrid material with a crystal-like wall structure. *Nature* **416**, 304–307 (2002).
12. B. J. Melde, B. T. Holland, C. F. Blanford, A. Stein, Mesoporous sieves with unified hybrid inorganic/organic frameworks. *Chem. Mater.* **11**, 3302–3308 (1999).
13. A. Ide, R. Voss, G. Scholz, G. A. Ozin, M. Antonietti, A. Thomas, Organosilicas with chiral bridges and self-generating mesoporosity. *Chem. Mater.* **19**, 2649–2657 (2007).
14. M. Ohashi, M. P. Kapoor, S. Inagaki, Chemical modification of crystal-like mesoporous phenylene-silica with amino group. *Chem. Commun.* 841–843 (2008).
15. S. Polarz, A. Kuschel, Preparation of a periodically ordered mesoporous organosilica material using chiral building blocks. *Adv. Mater.* **18**, 1206–1209 (2006).
16. K. Nakajima, I. Tomita, M. Hara, S. Hayashi, K. Domen, J. N. Kondo, A stable and highly active hybrid mesoporous solid acid catalyst. *Adv. Mater.* **17**, 1839–1842 (2005).
17. A. Ajayaghosh, Chemistry of squaraine-derived materials:Near-IR dyes, low band gap systems, and cation sensors. *Acc. Chem. Res.* **38**, 449–459 (2005).
18. A. Ajayaghosh, Donor–acceptor type low band gap polymers: Polysquaraines and related systems. *Chem. Soc. Rev.* **32**, 181–191 (2003).
19. S. Sreejith, P. Carol, P. Chithra, A. Ajayaghosh, Squaraine dyes: A mine of molecular materials. *J. Mater. Chem.* **18**, 264–274 (2008).
20. L. Beverina, P. Salice, Squaraine compounds: Tailored design and synthesis towards a variety of material science applications. *Eur. J. Org. Chem.* **2010**, 1207–1225 (2010).
21. R. R. Avirah, D. T. Jayaram, N. Adarsh, D. Ramaiah, Squaraine dyes in PDT: From basic design to in vivo demonstration. *Org. Biomol. Chem.* **10**, 911–920 (2012).
22. A. Ajayaghosh, E. Arunkumar, J. Daub, A highly specific Ca^{2+}-ion sensor: Signaling by exciton interaction in a rigid–flexible–rigid bichromophoric "H" foldamer. *Angew. Chem. Int. Ed.* **41**, 1766–1769 (2002).
23. E. Arunkumar, P. Chithra, A. Ajayaghosh, A controlled supramolecular approach toward cation-specific chemosensors: Alkaline earth metal ion-driven exciton signaling in squaraine tethered podands. *J. Am. Chem. Soc.* **126**, 6590–6598 (2004).

24. M. C. Basheer, S. Alex, K. G. Thomas, C. H. Suresh, S. Das, A squaraine-based chemosensor for Hg^{2+} and Pb^{2+}. *Tetrahedron* **62**, 605–610 (2006).
25. B.-L. Renard, Y. Aubert, U. Asseline, Fluorinated squaraine as near-IR label with improved properties for the labeling of oligonucleotides. *Tetrahedron Lett.* **50**, 1897–1901 (2009).
26. L. Beverina, M. Crippa, M. Landenna, R. Ruffo, P. Salice, F. Silvestri, S. Versari, A. Villa, L. Ciaffoni, E. Collini, C. Ferrante, S. Bradamante, C. M. Mari, R. Bozio, G. A. Pagani, Assessment of water-soluble π-extended squaraines as one- and two-photon singlet oxygen photosensitizers: Design, synthesis, and characterization. *J. Am. Chem. Soc.* **130**, 1894–1902 (2008).
27. H.-Y. Ahn, S. Yao, X. Wang, K. D. Belfield, Near-infrared-emitting squaraine dyes with high 2PA cross-sections for multiphoton fluorescence imaging. *ACS Appl. Mater. Interfaces* **4**, 2847–2854 (2012).
28. J. V. Ros-Lis, B. García, D. Jiménez, R. Martínez-Máñez, F. Sancenón, J. Soto, F. Gonzalvo, M. C. Valldecabres, Squaraines as fluoro–chromogenic probes for thiol-containing compounds and their application to the detection of biorelevant thiols. *J. Am. Chem. Soc.* **126**, 4064–4065 (2004).
29. S. Sreejith, K. P. Divya, A. Ajayaghosh, A near-infrared squaraine dye as a latent ratiometric fluorophore for the detection of aminothiol content in blood plasma. *Angew. Chem. Int. Ed.* **47**, 7883–7887 (2008).
30. P. Anees, S. Sreejith, A. Ajayaghosh, Self-assembled near-infrared dye nanoparticles as a selective protein sensor by activation of a dormant fluorophore. *J. Am. Chem. Soc.* **136**, 13233–13239 (2014).
31. S. Sreejith, X. Ma, Y. Zhao, Graphene oxide wrapping on squaraine-loaded mesoporous silica nanoparticles for bioimaging. *J. Am. Chem. Soc.* **134**, 17346–17349 (2012).
32. E. Arunkumar, C. C. Forbes, B. C. Noll, B. D. Smith, Squaraine-derived rotaxanes: Sterically protected fluorescent near-IR dyes. *J. Am. Chem. Soc.* **127**, 3288–3289 (2005).
33. J. M. Baumes, J. J. Gassensmith, J. Giblin, J.-J. Lee, A. G. White, W. J. Culligan, W. M. Leevy, M. Kuno, B. D. Smith, Storable, thermally activated, near-infrared chemiluminescent dyes and dye-stained microparticles for optical imaging. *Nat. Chem.* **2**, 1025–1030 (2010).
34. Y. Goto, S. Inagaki, Synthesis of large-pore phenylene-bridged mesoporous organosilica using triblock copolymer surfactant. *Chem. Commun.* 2410–2411 (2002).
35. B. Rác, P. Hegyes, P. Forgo, Á. Molnár, Sulfonic acid-functionalized phenylene-bridged periodic mesoporous organosilicas as catalyst materials. *Appl. Catal. A* **299**, 193–201 (2006).
36. M. Rat, M. H. Zahedi-Niaki, S. Kaliaguine, T. O. Do, Sulfonic acid functionalized periodic mesoporous organosilicas as acetalization catalysts. *Microporous Mesoporous Mater.* **112**, 26–31 (2008).
37. S. Shylesh, A. Wagener, A. Seifert, S. Ernst, W. R. Thiel, Mesoporous organosilicas with acidic frameworks and basic sites in the pores: An approach to cooperative catalytic reactions. *Angew. Chem. Int. Ed.* **49**, 184–187 (2010).
38. K. S. W. Sing, Reporting physisorption data for gas/solid systems with special reference to the determination of surface area and porosity. *Pure Appl. Chem.* **54**, 2201–2218 (1982).
39. X. Ma, S. Sreejith, Y. Zhao, Spacer intercalated disassembly and photodynamic activity of zinc phthalocyanine inside nanochannels of mesoporous silica nanoparticles. *ACS Appl. Mater. Interfaces* **5**, 12860–12868 (2013).
40. C. Li, M. Z. Hoffman, Oxidation of phenol by singlet oxygen photosensitized by the tris(2,2′-bipyridine)ruthenium(II) ion. *J. Phys. Chem. A* **104**, 5998–6002 (2000).
41. M. C. DeRosa, R. J. Crutchley, Photosensitized singlet oxygen and its applications. *Coord. Chem. Rev.* **233–234**, 351–371 (2002).
42. K. Jähnisch, V. Hessel, H. Löwe, M. Baerns, Chemistry in microstructured reactors. *Angew. Chem. Int. Ed.* **43**, 406–446 (2004).
43. J. C. McDonald, D. C. Duffy, J. R. Anderson, D. T. Chiu, H. Wu, O. J. A. Schueller, G. M. Whitesides, Fabrication of microfluidic systems in poly(dimethylsiloxane). *Electrophoresis* **21**, 27–40 (2000).
44. G. Leriche, G. Budin, L. Brino, A. Wagner, Optimization of the azobenzene scaffold for reductive cleavage by dithionite; development of an azobenzene cleavable linker for proteomic applications. *Eur. J. Org. Chem.* **2010** 4360–4364 (2010).
45. J. Gao, Y. He, F. Liu, X. Zhang, Z. Wang, X. Wang, Azobenzene-containing supramolecular side-chain polymer films for laser-induced surface relief gratings. *Chem. Mater.* **19**, 3877–3881 (2007).
46. M. A. O. Lourenço, R. Siegel, L. Mafra, P. Ferreira, Microwave assisted *N*-alkylation of amine functionalized crystal-like mesoporous phenylene-silica. *Dalton Trans.* **42**, 5631–5634 (2013).

Funding: This research was supported by the National Research Foundation (NRF), Prime Minister's Office, Singapore under its NRF Fellowship (NRF2009NRF-RF001-015) and Campus for Research Excellence and Technological Enterprise Programme–Singapore-Peking University Research Centre for A Sustainable Low-Carbon Future, as well as the Nanyang Technological University–A*STAR (Agency for Science, Technology and Research) Silicon Technologies, Centre of Excellence under grant no. 11235100003. **Author contributions:** P.B., S.S., P.A., A.A., and Y.Z. designed and planned this project. P.B., S.S., and P.A. carried out the synthesis and characterizations of the materials and performed the photo-oxidation of phenol. N.V.M. and Y.K. were involved in the design and fabrication of the microfluidic device. P.B., S.S., P.A., A.A., and Y.Z. cowrote this paper, and all authors discussed the results and commented on the manuscript. **Competing interests:** The authors declare that they have no competing interests. **Data and materials availability:** The authors will make data available upon request.

Submitted 25 March 2015
Accepted 5 June 2015
Published 11 September 2015
10.1126/sciadv.1500390

Citation: P. Borah, S. Sreejith, P. Anees, N. V. Menon, Y. Kang, A. Ajayaghosh, Y. Zhao, Near-IR squaraine dye–loaded gated periodic mesoporous organosilica for photo-oxidation of phenol in a continuous-flow device. *Sci. Adv.* **1**, e1500390 (2015).

ScienceAdvances

Near-IR squaraine dye–loaded gated periodic mesoporous organosilica for photo-oxidation of phenol in a continuous-flow device

Parijat BorahSivaramapanicker SreejithPalapuravan AneesNishanth Venugopal MenonYuejun KangAyyappanpillai AjayaghoshYanli Zhao

Sci. Adv., 1 (8), e1500390. • DOI: 10.1126/sciadv.1500390